



LAWRENCE  
LIVERMORE  
NATIONAL  
LABORATORY

# Using fully coupled hydro-geomechanical numerical test bed to study reservoir stimulation with low hydraulic pressure

P. Fu, S. M. Johnson, C. R. Carrigan

January 20, 2012

37th Stanford Geothermal Workshop  
Stanford, CA, United States  
January 30, 2012 through February 1, 2012

## **Disclaimer**

---

This document was prepared as an account of work sponsored by an agency of the United States government. Neither the United States government nor Lawrence Livermore National Security, LLC, nor any of their employees makes any warranty, expressed or implied, or assumes any legal liability or responsibility for the accuracy, completeness, or usefulness of any information, apparatus, product, or process disclosed, or represents that its use would not infringe privately owned rights. Reference herein to any specific commercial product, process, or service by trade name, trademark, manufacturer, or otherwise does not necessarily constitute or imply its endorsement, recommendation, or favoring by the United States government or Lawrence Livermore National Security, LLC. The views and opinions of authors expressed herein do not necessarily state or reflect those of the United States government or Lawrence Livermore National Security, LLC, and shall not be used for advertising or product endorsement purposes.

## USING FULLY COUPLED HYDRO-GEOMECHANICAL NUMERICAL TEST BED TO STUDY RESERVOIR STIMULATION WITH LOW HYDRAULIC PRESSURE

Pengcheng Fu, Scott M. Johnson, and Charles R. Carrigan

Atmospheric, Earth, and Energy Division, Lawrence Livermore National Laboratory  
7000 East Ave., L-286  
Livermore, CA 94550, USA  
e-mail: fu4@llnl.gov

### **ABSTRACT**

Papers should follow standard technical paper format, an abstract followed by the more detailed presentation. The abstract should be typed on this area of the first page, with the presentation following after two lines of space.

### **INTRODUCTION**

Geological formations in crystalline rocks with low initial permeability can be hydraulically stimulated to create enhanced (or engineered) geothermal reservoirs with enhanced permeability and thereby improved heat production efficiency. The conceptual model for hydraulic stimulation that is most commonly referred to depicts the following process. When fluid pressure exceeds the minimum principal stress in the rock formation, new hydraulic fractures initiate and propagate along the plane that is perpendicular to the minimum principal stress direction. These new hydraulic fractures will intersect existing natural fractures in the formation and form an interconnected fracture network, through which fluid in the production phase can flow from the injection well to production well(s) and bring heat from the hot rocks covered by this network.

A concern over the process described in this conceptual model is that once a hydraulic fracture (termed primary fracture here) is opened, the conductivity within this fracture from the injection point to the fracture front is much higher than the neighboring fractures that are still closed. Meanwhile, the high fluid pressure in this open fracture creates a “stress shadow” around this fracture, which increases the rock matrix compressive stress experienced by closed fractures. The direct consequence of these two effects is that this open fracture will continue to grow at a relatively high rate, thereby further strengthening these effects, whereas the neighboring closed fracture may never be able to open and subsequently compete with the primary fracture. This is true regardless whether the

primary fracture is a newly created hydraulic fracture or a existing fracture that happens to be oriented normal to the minimum principal stress. In this scenario, only one fracture (the primary fracture) can be stimulated. Even though it is possible to obtain high permeability between the injection well and the production well through this primary fracture, only a small volume in the reservoir around this fracture is stimulated, which is highly undesired for enhanced geothermal system (EGS) stimulation. It is possible to stimulate multiple fractures and create interconnected fracture network using technologies such as horizontal drilling with staged fracking, but such technologies are expensive and more applicable to shale gas production than to EGS.

An alternative stimulation strategy is to stimulate the reservoir at a fluid pressure lower than the minimum principal stress in the rock matrix. No new fracture will be created and no fracture will be completely open. In this scenario, instead of stimulate a single fracture, the fracture network which must already be interconnected prior to the stimulation will be stimulated by “hydro-shearing” (Willis-Richards et al., 1996). This paper investigates the mechanisms of low pressure hydraulic stimulation using a fully coupled hydro-geomechanical numerical test bed developed at the Lawrence Livermore National Laboratory. The numerical algorithms in this numerical test bed, which originally focuses on high-pressure hydraulic fracturing, have been described elsewhere (Fu et al., 2011). In this paper, we describe the modifications to the original algorithms that enable the simulation of low pressure stimulation in this paper, as well as various numerical examples on low pressure stimulation.

### **STRESS SHADOWING CONSIDERATION**

First, we quantitatively evaluate the evolution of stress shadowing, namely the increase of rock matrix stress as fluid pressure in a fracture increases. Consider an infinite array of parallel fractures with infinite length as a highly idealized scenario that enables a closed-form solution to be obtained, as

illustrated in Figure 1. The distance between any two neighboring fractures is  $H$ . Initially the fluid pressure in these fractures is  $P_F=0$  and the rock matrix stress normal to the fractures is  $\sigma_{M0}$ . As the fractures are simultaneously pressurized with a fluid, they will begin to dilate and the rock matrix stress  $\sigma_M$  will increase accordingly. The effective normal stress along these fractures

$$\sigma'_J = \begin{cases} \sigma_M - P_F & \text{if } \sigma_M > P_F \\ 0 & \text{otherwise} \end{cases} \quad (1)$$

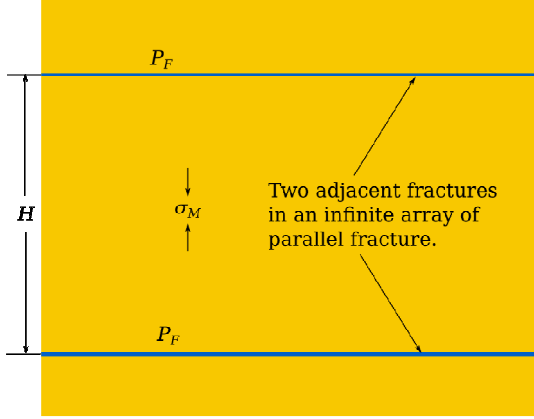


Figure 1: Two adjacent fractures in an infinite array of parallel fractures.

Note that  $\sigma_M$  is not a constant, but a function of  $\sigma_{M0}$  and  $P_F$ . Assume under the initial condition (effective normal stress being  $\sigma_{Mi}$ ) the mechanical aperture width is  $w_i$ ; at arbitrary effective joint stress  $\sigma'_J$  the mechanical aperture width becomes  $w$ . We define the secant unloading joint stiffness to be

$$\bar{k}_n = \frac{\sigma_{M0} - \sigma'_J}{w(\sigma'_J) - w_i} \quad (2)$$

The normal stiffness of a joint  $k_n$  is conventionally defined using the zero-normal stress state as the reference state, whereas we use the zero-fluid pressure state as the reference. The compression experienced by the rock body between two neighboring fractures due to a matrix stress increase from  $\sigma_{Mi}$  to  $\sigma_M$  should be the same as the joint dilation due to the corresponding effective stress change from  $\sigma_{Mi}$  to  $\sigma'_J$ , namely

$$w(\sigma'_J) - w_i = \frac{(\sigma_M - \sigma_{Mi})H}{E'} \quad (3)$$

where  $E'$  is the confined stiffness of the rock matrix as

$$E' = \frac{E(1-\nu)}{(1-2\nu)(1+\nu)} \quad (4)$$

with  $E$  and  $\nu$  being the Young's modulus and Poisson's ratio of the rock, respectively. We introduce a length scale

$$\bar{h}_n = E' / \bar{k}_n \quad (5)$$

so that the closure of the joint between the reference stress state and the current effective stress state is the same as the compression of a layer of virtual rock mass of thickness  $\bar{k}_n$  experiencing the same stress change.

By plugging equations (1) and (2) into equation (3), we can obtain the increment of rock matrix stress  $\Delta\sigma_M = \sigma_M - \sigma_{Mi}$  as

$$\Delta\sigma_M = \begin{cases} P_F / (1 + H / \bar{h}_n) & \text{if } P_F \leq \sigma_{Mi} (1 + \bar{h}_n / H) \\ P_F - \sigma_{Mi} & \text{otherwise} \end{cases} \quad (6)$$

which indicates that the fracture will be completely open if the fluid pressure is higher than a threshold value of  $\sigma_{Mi} (1 + \bar{h}_n / H)$ . When the fracture is still partially closed, the rock matrix stress increment is only a portion of the fluid pressure increment. A survey of rock mechanics literature found that  $\bar{h}_n$  is generally within the range between tens to hundreds of millimeters for interlocked rocks compressed with a stress level typical of hydraulic stimulation applications. If the fracture spacing is in the range of a few meters to tens of meters, then the rock matrix stress increment is a relatively small percentage of the fluid pressure increment. Therefore, the stress shadowing effects for partially closed fractures can generally be ignored. We term this scenario "joint stiffness-dominated" regime for fracture flow.

On the other hand, however, as the fluid pressure exceeds the threshold value and the fractures are completely open, the opening of the fracture will not be governed by joint stiffness, but by the deformation in the rock matrix instead. Under this condition, the stress shadowing effects mentioned in the first section dictates that a primary fracture will emerge and suppress the pressure propagation in neighbor fractures.

## COUPLING JOINT MODEL WITH FLOW SOLVER

In order to investigate fluid pressure propagation in the joint stiffness-dominated regime in an arbitrary fracture network, we use the numerical model for hydraulic fracturing developed at the Lawrence Livermore National Laboratory (LLNL). This fully coupled hydro-geomechanical model has been described elsewhere (Fu et al., 2011) and will not be repeated here. However, the original model was formulated for the scenarios where the fractures are completely open. To simulate the cases with partially closed fractures, some modifications are necessary. The weak stress shadowing effect allows us to

directly incorporate joint closure models into the finite volume flow solver.

Fractures are discretized into interconnected flow cells in the flow solver. The permeability of each flow cell is a function of the hydraulic aperture width and the fluid storage volume of a cell is related to the mechanical aperture size. It is well known that the hydraulic aperture width is highly correlated with the mechanical aperture size as effective stress evolves, with the former generally smaller than the latter (references). However, their difference is ignored in this preliminary study. In each time step of solving the network flow, the fluid mass into and out of each flow cell is calculated and subsequently, the fluid mass in each cell is updated. Fluid pressure in each cell is calculated using the following equation-of-state

$$P_F = \begin{cases} K_F \left( 1 - \frac{\rho_{ref} L_C w}{m_C} \right) & \text{if } m_C / L_C w \geq \rho_{ref} \\ P_{vap} & \text{if } m_C / L_C w < \rho_{ref} \end{cases} \quad (7)$$

where  $K_F$  is the bulk modulus of the fluid;  $\rho_{ref}$  is the reference density of this fluid, namely the density at zero or the datum pressure;  $L_C$  is the length (area in 3D) of the fluid cell and  $w$  is the aperture width, so  $L_C w$  is the fluid storage volume of the cell;  $m_C$  is the fluid mass in this cell;  $P_{vap}$  is the temperature-dependent vapor pressure of this fluid which can be considered to be zero for the purpose of hydraulic stimulation modeling as the pumping pressure is many orders of magnitude higher than the vapor pressure. In the original model, the aperture width is calculated based on the deformation of the rock mass through a finite element solver. In the current study, instead we adopt the well known closure model by Bandis et al., which relates the aperture width  $w$  and joint effective normal stress as

$$\sigma' = \frac{w_{max} - w}{a - b(w_{max} - w)} \quad (8)$$

where  $w_{max}$  is the aperture width at the zero-effective stress state, which is essentially the maximum joint closure in the original joint model;  $a$  and  $b$  are two material-specific constant. We plug equations (7) and (8) into equation (1) and obtain

$$\sigma_M - K_F \left( 1 - \frac{\rho_{ref} L_C w}{m_C} \right) = \frac{w_{max} - w}{a - b(w_{max} - w)} \quad (9)$$

which can be solved as

$$w = w_{max} - \frac{Aa + Bb + 1 - [(Aa + Bb + 1)^2 - 4AaBb]^{0.5}}{2Ab} \quad (10)$$

where  $A = K_F \rho_{ref} L_C / m_C$  and  $B = \sigma_M - K_F + A w_{max}$  are two constants to simplify the expression of the equations. With this equation, we can directly calculate the aperture width at each time step from the updated fluid mass and then obtain the fluid pressure using equation (7). The finite element solid solver is not required for joint stiffness-dominated fluid flow.

## FLOW IN A SINGLE FRACTURE

We investigate fluid flow in a single fracture in this section. Because the strong coupling between fluid pressure, aperture volume, and aperture permeability, closed-form solutions cannot be derived.

A 100 meter long straight fracture is considered and it is discretized into 1,000 flow cells with  $L_C = 0.1$  m. In the initial condition where no fluid exists in the fracture, the normal stress along the fracture  $\sigma_n = 10$  and we ignore the total normal stress change due to pressurization of the fracture. In this state, the aperture width  $w_i = 0.01$  mm whereas  $w_{max} = 0$  corresponding to the zero-effective stress state. The closing behavior of the fracture is anchored by these two states and we can back-calculate the two constants in the joint model as

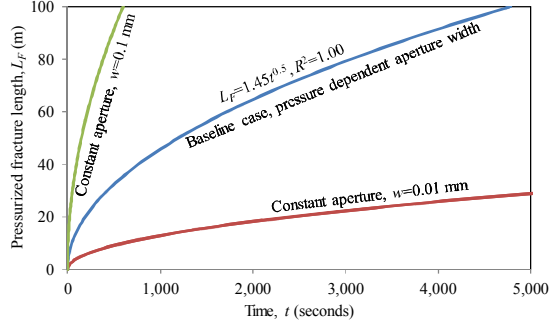
$$a = w_{max} \frac{w_{max} - w_i}{\sigma_n w_i} \quad \text{and} \quad b = \frac{w_{max} - w_i}{\sigma_n w_i} \quad (11)$$

The dynamic viscosity, bulk modulus ( $K_F$ ), and reference density ( $\rho_{ref}$ ) of the fluid are 0.001 Pa·s, 2.2 GPa, and 1000 kg/m<sup>3</sup>, respectively. All the above parameters remain the same for all the numerical examples in this paper unless stated otherwise.

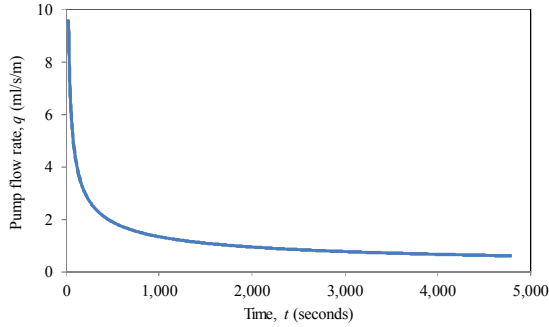
In the baseline scenario, we start pumping fluid with pressure  $P_{F0} = 10$  MPa into the fracture at time  $t = 0$ . This is also the highest fluid pressure allowed by the joint stiffness-dominated regime. The length of the fracture that is pressurized by fluid  $L_F$  as a function of  $t$  is shown in Figure 2(a). A regression analysis finds that  $L_F$  is linearly proportion to the square root of  $t$ , with the regression equation and a perfect  $R^2$  value shown in the figure. For an ideal case where the aperture width is a constant regardless of the fluid pressure, a closed-form solution exist between  $L_F$  and  $t$  as

$$L_F = w \left( \frac{P_0 t}{6\mu} \right)^{1/2} \quad (12)$$

which also indicates that  $L_F$  is a linear function of the square root of  $t$ . In Figure 2(a), two scenarios with pressure-independent aperture widths 0.1 mm and 0.01 mm are plotted. Since these two aperture widths are the upper and lower bounds of the aperture width in the baseline case, it is not surprising to see the propagation speed of the baseline case is somewhere between these two ideal cases.



(a)



(b)

Figure 2: Numerical simulation results for the baseline single fracture. (a).

The flow rate  $q$  at the pumping end of the fracture decreases as the fluid front propagates, as shown in Figure 2(b). This phenomenon has an important implication for the stimulation of a fracture network instead of a single primary fracture. It indicates that as the stimulation progresses, it will be harder and harder to pump fluid into a single fracture. The flow tends to find alternative route, thereby stimulating other fractures in the network. On the other hand, if an open primary fracture has developed, the flow rate into this fracture increases as this fracture grows if the pump pressure remains constant. This single fracture will consume most of the flow volume and make the stimulation of other fractures more difficult.

Two more simulations for the same single fracture but with lower pumping pressures, 5 MPa and 2 MPa, were performed and the results are shown in Figure 3. The effect of pumping pressure on the fluid front propagation rate is very significant. For all the three pumping pressures,  $L_F$  is always a linear function of the square root of time. We also implemented some

other forms of the relationship between the effective normal stress and the aperture width in addition to the Bandis-Barton model, and found that this square root grow rate relationship is always valid.

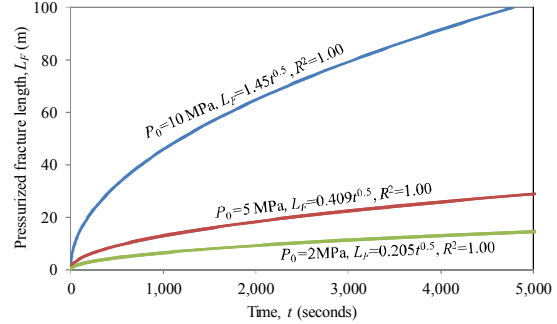


Figure 3: The effects of pumping pressure  $P_0$  on the growth rate of  $L_F$ .

### SELF-PROPPING THROUGH SHEAR DILATION

It is believed that a fracture network can be stimulated by the mechanism of shear dilation under the following conditions: 1) There exists significant shear stress long the fractures; and 2) the fluid pressure is high enough to induce shear slipping of the fractures as a result of the reduced effective stress. Predicting the amount of shear dilation is a challenging task, primarily due to the lack of experiment data that enable characterization of joint behaviors along the complex stress paths associated with hydraulic stimulation and drawdown. The following simple phenomenological empirical model is used in this study to represent the most important shear dilation behaviors associated with low pressure stimulation.

We introduce a variable, termed the stimulation factor  $S$  to quantify the extent to which a fracture has been stimulated through shear dilation. The aperture width is a function of not only the compressive effective stress  $\sigma'$ , but also this stimulation factor  $S$ . If we assume the effects of  $\sigma'$  and those of  $S$  can be decoupled,  $S$  becomes a multiplier of the original joint model as

$$w = w(\sigma', S) = Sw(\sigma')$$

In the unstimulated state,  $S=S_0=1$ . We denote the three parameters in the joint model in this state as  $w_{max0}$ ,  $a_0$  and  $b_0$ , and the evolution of these parameters with  $S$  is as  $w_{max} = w_{max0}S$  and  $a = a_0S$  while  $b$  is a constant as  $b=b_0$ . We define the “excessive” shear stress along a fracture to be  $\tau' = \tau_0 - \sigma'v$ , where  $\tau_0$  is the shear stress along the fracture in the initial state without hydraulic pressure and  $v$  is coefficient of friction of the fracture. The stimulation factor  $S$  is assumed to be

related to the greatest excessive shear stress  $\tau'_{max}$  ever achieved by the fracture

$$S = \begin{cases} 1 + \tau'_{max} (S_{max} - 1) / \tau'_s & \text{if } \tau'_{max} < \tau'_s \\ S_{max} & \text{otherwise} \end{cases}$$

where  $S_{max}$  is the upper limit of  $S$  and  $S$  reaches  $S_{max}$  at excessive shear stress  $\tau'_s$ . The above formulation dictates that an increase of the excessive shear stress can induce increase of  $S$ , but a decrease of  $\tau'$  has no effect on  $S$ . In other words, the stimulation effects induced by the increase of fluid pressure will not be reversed when the pressure decreases after the stimulation. However, the aperture size is still a function of the effective stress as dictated by equation (8). The main effect of stimulation by shear dilation is to change the values of the constants in equation (8).

### **NUMERICAL EXAMPLE: STIMULATION OF A NATURAL FRACTURE NETWORK**

In this section, we exercise the numerical model on a virtual reservoir. As shown in Figure 4, the simulation domain is 320 m wide (x from -160 m to 160 m) and 240 m tall (y from 0 to 240 m). There are two sets of joints (existing natural fractures) in this reservoir. The horizontal set has orientation angles with a uniform distribution between  $10^\circ$  and  $30^\circ$  where as the vertical set has orientation angles between  $80^\circ$  and  $100^\circ$ . Note that this 2D simulation domain should be considered as a plan view of the reservoir, so the term “vertical” actually refers to the direction within the image. All the fractures have lengths between 20 m and 60 m and the total length of fractures in the two sets are 8,300 m and 8,700 m respectively. The injection well is located near the middle point of the lower boundary of the domain as shown in Figure 4, so the simulation is on half of the reservoir. The location of the production well is shown in Figure 4. The far field in situ stress applied is  $\sigma_{xx}=10$  MPa,  $\sigma_{yy}=14$  MPa, and  $\sigma_{xy}=0$ . Although no far field shear stress is applied, since the fractures usually do not align with the coordinate system, shear stress with varying shear stress dependent on the orientation angle exist along these fractures. Joint model parameters used are shown in Table 1 and parameters for the fluid phase are the same as the numerical examples for single fractures..

Table 1: Model parameters used in this study.

Parameter	Value
$w_{max0}$	0.2 mm
$w_{i0}$	0.02 mm
$\tau'_s$	3 MPa
$S_{max}$	3.0
$\nu$	0.7

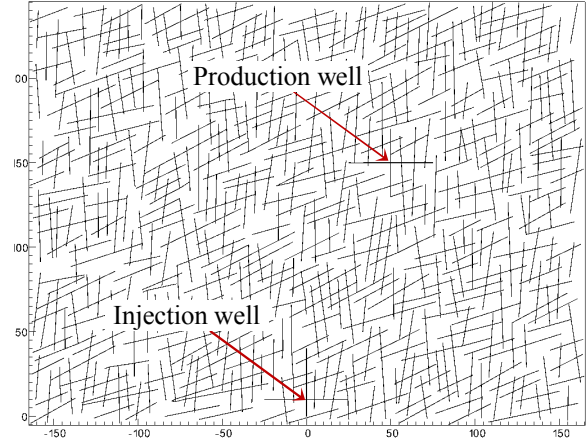


Figure 4: The effects of pumping pressure  $P_0$  on the growth rate of  $L_F$ .

The injection pressure at the injection well is 10 MPa, the same as the minimal preincipal stress. The portions of the fracture network that is pressurized (with non-zero fluid fracture) at 20,000 seconds (5.6 hours) and 100,000 seconds (28 hours) after the injection has started are shown in Figure 5.

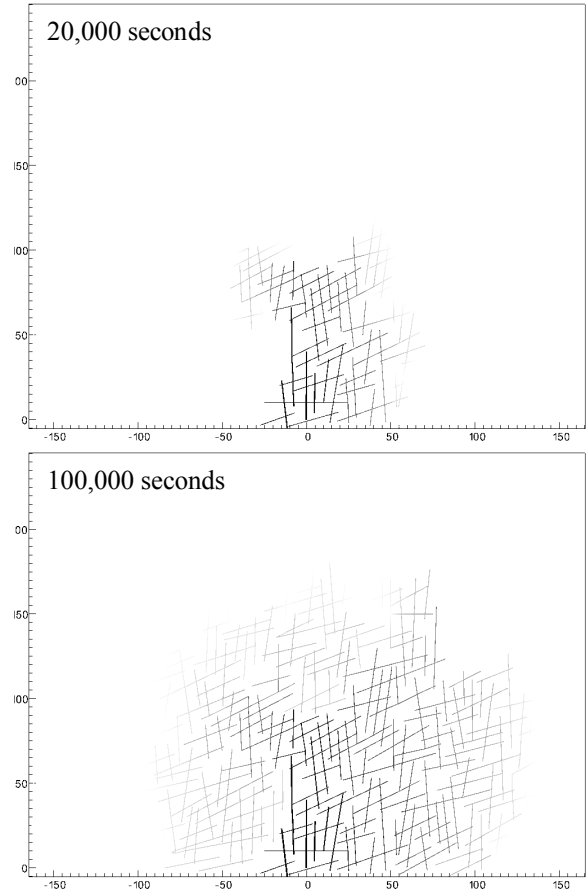


Figure 5: Pressurized fracture network 20,000 and 100,000 seconds after stimulation.

We simulate four scenarios (A to D) that share the same stimulation process in the first 100,000 seconds as described above but with different operations after 100,000 seconds. For cases A through C, we start pumping into the production well at 10 MPa fluid pressure from 100,000 seconds to 125,000 seconds. The objective is to stimulate the fractures near the production well. The difference between these three cases is the back pressure we use in the production case, being 0, 2 MPa, and 4 MPa for cases A, B, and C, respectively. A higher back pressure can increase the aperture width and permeability in the near-well region but on the other hand, it also decreases the pressure gradient from the injection well and the production well. In case D, we do not stimulate the region around the production well and we directly apply 4 MPa of back pressure at 100,000 seconds.

The flow rates at the two wells for case A are shown in Figure 6. Negative flow rate means flow from the well into the reservoir and positive value means flow from the reservoir to the well. Because this is a 2D model, the flow rate is for unit-thickness reservoir. From the beginning of the stimulation ( $t=0$ ) to 100,000 seconds, the absolute flow rate at the injection well continues to decrease, similar to what the single fracture model has shown. The fluid front reaches the production well at approximately 50,000 seconds, and fluid starts to flow out from that well, which is an artifact of the zero-pressure boundary condition given at the well. Fluid flow into the production well between  $t=100,000$  and  $t=125,000$  seconds during the stimulation through the production well. Once we lower the pressure to the back pressure (0 for case A), fluid starts to flow back into the well. The flow rate in the beginning is high due to the high pressure that has built up during production well stimulation, and it soon reaches a relatively steady level when most of the fluid is supplied from the injection well. We terminate the simulation at 300,000 seconds because the fluid front has reached the boundary of the simulation domain. At this moment, the injection rate is still slowly decreasing and the production rate is slowing increasing. The flow rate at  $t=300,000$  seconds for all four scenarios are summarized in Table 2.

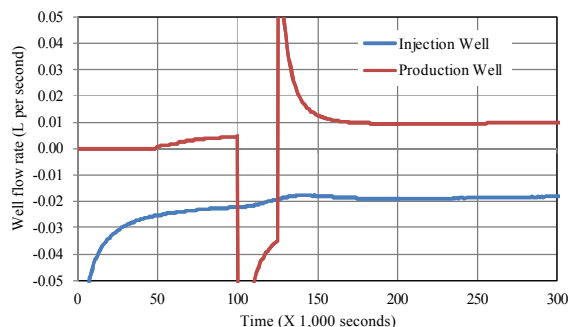


Figure 6: Flow rate at the two wells in scenario A.

Table 2: Absolute flow rate at  $t=300,000$  seconds.

Scenario	Injection (L/s)	Production (L/s)
A	0.0183	0.00991
B	0.0197	0.00913
C	0.0197	0.00779
D	0.0193	0.00720

The fluid recovery ratios (production flow rate divided by injection rate) for the four scenarios are 54%, 46%, 40%, and 37%, respectively. The benefit of production well stimulation is apparent, but the back pressure seems to not only reduce flow rate but also decrease recovery rate. Adding more production wells should increase the recovery ratio, but this is to be studied in the future.

## SUMMARY

In this study, we investigate the use of a numerical test bed to study the stimulation of existing fracture networks with relatively low hydraulic pressure. We found that in this regime, the coupling between the flow and the solid phase can be considered local and the numerical model can be greatly simplified. The results show that low pressure stimulation can indeed stimulate the entire network, instead of a primary fracture as in high pressure stimulation. This paper only documents our initial effort, and more realistic scenarios are to be studied.

## AUSPICES AND ACKNOWLEDGEMENTS

The authors gratefully acknowledge the Geothermal Technologies Program of the US Department of Energy for support of this work under the Enhanced Geothermal Systems Program. The authors also would like to acknowledge their collaborators at the Lawrence Livermore National Laboratory. This work was performed under the auspices of the U.S. Department of Energy by Lawrence Livermore National Laboratory under Contract DE-AC52-07NA27344.

## REFERENCES

- The Future of Geothermal Energy: Impact of Enhanced Geothermal Systems (EGS) on the United States in the 21<sup>st</sup> Century* (2006). Research report by an MIT-led interdisciplinary panel.
- Adachi, J., Siebrits, E., Peirce, A., and Desroches J. (2007), "Computer simulation of hydraulic fractures," *International Journal of Rock Mechanics and Mining Sciences*, **44**, 739-757.
- Barton, N., Bandis, S., and Bakhtar, K. (1985), "Strength, deformation and conductivity coupling of rock joints," *International Journal of*

*Rock Mechanics and Mining Sciences & Geomechanics Abstracts*, **22**, 121-140.

- Block, G., Rubin, M.B., Morris, J., and Berryman, J.G. (2007), "Simulations of dynamic crack propagation in brittle materials using nodal cohesive forces and continuum damage mechanics in the distinct element code LDEC," *International Journal of Fracture*, **144**, 131-147.
- Camacho, G., and Ortiz, M. (1996), "Computational modelling of impact damage in brittle materials," *International Journal of Solids and Structures*, **33**, 2899-2938.
- Detournay, E. (2004), "Propagation regimes of fluid-driven fractures in impermeable rocks," *International Journal of Geomechanics*, **4**, 35-45.
- Geertsma, J., and de Klerk, F. (1969), "A rapid method of predicting width and extent of hydraulically induced fractures," *Journal of Petroleum Technology*, **21**, 1571-1581.
- Huttert, K.M., and Willis, D.G. (1957), "Mechanics of hydraulic fracturing," *Transactions of The American Institute of Mining And Metallurgical Engineers*, **210**, 153-163.
- Johnson, J.W., Nitao, J.J., and Knauss, K.G. (2004), "Reactive transport modeling of CO<sub>2</sub> storage in saline aquifers to elucidate fundamental processes, trapping mechanisms and sequestration partitioning", *Geological Storage of Carbon Dioxide*, S. J. Baines and R. H. Worden, Editors. Geological Society, London: London, 107-128.
- Johnson, S.M., and Morris, J.P. (2009), "Modeling hydraulic fracturing for carbon sequestration applications," *the 43<sup>rd</sup> US Rock Mechanics Symposium and the 4<sup>th</sup> US-Canada Rock Mechanics Symposium*, Asheville, NC, ARMA 09-30.
- Johnson, S.M., and Hao, Y. (2010), "Upscaling of thermal transport properties in enhanced geothermal systems" *Fall Meeting of the American Geophysical Union*, San Francisco, CA, Dec. 12-17.
- McClure, M.W., and Horne, R.N. (2010), "Discrete fracture modeling of hydraulic stimulation in enhanced geothermal systems," *Proceedings of the 35th Workshop on Geothermal Reservoir Engineering*, SGP-TR-188.
- Morris, J.P., Rubin, M.B., Block, G.I., and Bonner, M.P. (2006), "Simulations of fracture and fragmentation of geologic materials using combined FEM/DEM analysis," *International Journal of Impact Engineering*, **33**, 463-473.
- Morris, J.P., and Johnson S.M. (2009), "Dynamic simulations of geological materials using combined FEM/DEM/SPH analysis," *Geomechanics and Geoengineering: An International Journal*, **4**, 91-101.
- Nitao, J.J. (1998), *Reference Manual for the NUFT Flow and Transport Code*, Version 2.0. Lawrence Livermore National Laboratory: Livermore, CA.
- Nordgren, R.P. (1972), "Propagation of a vertical hydraulic fracture," *Society of Petroleum Engineers Journal*, **12**, 306-314.
- Perkins, T.K., and Kern, L.R. (1961), "Widths of hydraulic fractures," *Journal of Petroleum Technology*, **13**, 937-949.
- Xu, X.P., and Needleman, A. (1994), "Numerical simulations of fast crack growth in brittle solids," *Journal of the Mechanics and Physics of Solids*, **42**, 1397-1434.